ACS APPLIED MATERIALS & INTERFACES

Research Article

www.acsami.org

Enhancing the Lithium Ion Conductivity in Lithium Superionic Conductor (LISICON) Solid Electrolytes through a Mixed Polyanion Effect

Yue Deng,[†,‡,§,∥] Christopher Eames,[‡,§] Benoit Fleutot,[†,∥] Rénald David,[†,∥] Jean-Noël Chotard,[†,∥] Emmanuelle Suard,[⊥] Christian Masquelier,*[,†,§,∥] and M. Saiful Islam*[,‡,§]

[†]Laboratoire de Réactivité et Chimie des Solides (UMR CNRS 7314), Université de Picardie Jules Verne, 33 rue Saint Leu, 80039 Amiens Cedex, France

[‡]Department of Chemistry, University of Bath, Bath BA2 7AY, United Kingdom

[§]ALISTORE European Research Institute, FR CNRS 3104, 80039 Amiens Cedex, France

[∥]Réseau sur le Stockage Électrochimique de l'Énergie (RS2E), FR CNRS 3459, 80039 Amiens, France

[⊥]Institut Laue-Langevin, 71 Avenue des Martyrs, F-38000 Grenoble, France

Supporting Information

ABSTRACT: Lithium superionic conductor (LISICON)-related compositions $Li_{4\pm x}Si_{1-x}X_xO_4$ (X = P, Al, or Ge) are important materials that have been identified as potential solid electrolytes for all solid state batteries. Here, we show that the room temperature lithium ion conductivity can be improved by several orders of magnitude through substitution on Si sites. We apply a combined computer simulation and experimental approach to a wide range of compositions (Li_4SiO_4, $Li_{3.75}Si_{0.75}P_{0.25}O_4$, $Li_{4.25}Si_{0.75}Al_{0.25}O_4$, $Li_4Al_{0.33}Si_{0.33}P_{0.33}O_4$, and $Li_4Al_{1/3}Si_{1/6}Ge_{1/6}P_{1/3}O_4$) which include new doped materials. Depending on the temperature, three different Li^+ ion diffusion mechanisms are observed. The polyanion mixing introduced by substitution lowers the temperature at which the transition to a superionic state with high Li^+ ion conductivity occurs. These insights help to rationalize the mechanism of the lithium ion conductivity enhancement and provide strategies for designing materials with promising transport properties.

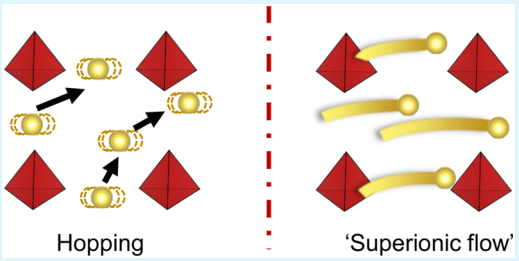

KEYWORDS: *energy storage, solid electrolyte, LISICON, diffusion mechanism, mixed polyanion effect*

1. INTRODUCTION

Lithium ion batteries are widely used in electric vehicles and portable devices.[1−5] However, owing to various intrinsic drawbacks of liquid electrolytes (for example, chemical and thermal instability and complex reactions at the solid/liquid interface), other technologies with better performance for specific applications are required. Among various electrochemical energy storage devices, all solid state batteries (ASSBs) have been proposed to provide improved chemical and electrochemical stability (wide potential window), greater safety, and easier device fabrication.[6−12]

The search for new, stable, and highly conducting solid electrolytes has increased significantly in recent years. Considerable research efforts have been carried out in exploring crystal structural families with high ionic conductivity, including the sodium superionic conductor (NASICON; e.g., $Na_3Zr_2Si_2PO_{12}$),[13−16] lithium superionic conductor (LISICON; e.g., γ-Li_3PO_4),[17−21] and thio-LISICON[22−25] garnets (e.g., $Li_7La_3Zr_2O_{12}$)[26,27] and related structures.[28−32] Among these structural families, the compositions $Li_{10}GeP_2S_{12}$ (10 mS/cm at 25 °C) and $Li_{9.54}Si_{1.74}P_{1.44}S_{11.7}Cl_{0.3}$ (25 mS/cm at 25 °C) reported by Kanno et al. present the highest ionic conductivities to date.[6,25] However, sulfide chemistry can be challenging in terms of its high sensitivity to moisture.[33−35] It is believed that the reproducible synthesis of phase pure materials will be a particular issue that will be difficult to overcome. In contrast, oxide-based LISICON materials can be obtained from traditional solid state reactions and present fewer air-sensitivity issues. Previous studies show that the formation of solid solutions (such as $Li_{4-x}Si_{1-x}P_xO_4$ or $Li_{4+x}Si_{1-x}Al_xO_4$) can significantly improve the ionic conductivity.[20,36−42] However, there is limited work on additional doping of these LISICON systems.

The mechanism for such drastic enhancement of conductivity in the solid solution compositions is considered to be caused by the increased concentration of defects which act as charge carriers. Our previous work revealed an interstitialcy or knock-on type mechanism in the case of lithium ion diffusion in $Li_{3.5}Si_{0.5}P_{0.5}O_4$ at 573 K.[20] However, the influence of the polyanion groups (e.g., SiO_4, PO_4) has not been discussed in

Received: November 11, 2016
Accepted: January 27, 2017
Published: January 27, 2017

DOI: 10.1021/acsami.6b14402
ACS Appl. Mater. Interfaces 2017, 9, 7050−7058

detail. In particular, there is limited work on compositions with more than two types of polyanion groups. For the composition $Li_{4.25}Si_{0.75}Al_{0.25}O_4$, previous work has reported that this material crystallizes in a LISICON structure.[43] However, detailed crystallographic information, e.g., Li atomic positions and site occupancy, is still lacking. For $Li_4Al_{0.33}Si_{0.33}P_{0.33}O_4$, to the best of our knowledge, no previous synthesis and characterization work has been reported. Such crystal structural information is important to aid understanding of ion diffusion mechanisms at the atomistic scale.

In this study, we investigate the temperature dependence of the crystal structure and ion diffusion mechanism, and whether the coexistence of various XO_4 tetrahedra ($(SiO_4)^{4-}$, $(PO_4)^{3-}$, and $(AlO_4)^{5-}$) within a given structure leads to lower lithium ion transport barriers similar to the "mixed anion effect" reported in polymer and glass-ceramic systems.[44−47] We synthesized, characterized, and modeled a series of compositions (Li_4SiO_4, $Li_{3.75}Si_{0.75}P_{0.25}O_4$, $Li_{4.25}Si_{0.75}Al_{0.25}O_4$, $Li_4Al_{0.33}Si_{0.33}P_{0.33}O_4$, and $Li_4Al_{1/3}Si_{1/6}Ge_{1/6}P_{1/3}O_4$) which are formed through cationic substitution on the Si^{4+} site of the parent LISICON-like Li_4SiO_4 structure (see Figure 1 for compositional relations).

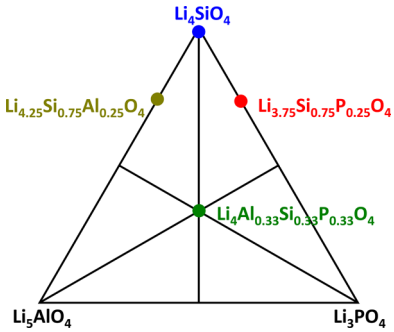

Figure 1. Phase diagram showing the compositions studied (Li_4SiO_4 (blue), $Li_{3.75}Si_{0.75}P_{0.25}O_4$ (red), $Li_{4.25}Si_{0.75}Al_{0.25}O_4$ (dark yellow), and $Li_4Al_{0.33}Si_{0.33}P_{0.33}O_4$ (green)) and their relation to the three parent compositions (Li_4SiO_4, Li_5AlO_4, and Li_3PO_4).

This work represents the first successful doping of more than three elements on the silicon site and the first application of van Hove analysis of these systems, which sheds new light on the nature of the superionic transition in LISICON materials. The findings here are directly transferable to the high conductivity sulfide-based thio-LISICON systems and offer design strategies to further improve the conductivity.

2. METHODS

2.1. Synthesis, Structural, and Chemical Characterization. Li_4SiO_4, $Li_{3.75}Si_{0.75}P_{0.25}O_4$, $Li_{4.25}Si_{0.75}Al_{0.25}O_4$, and $Li_4Al_{0.33}Si_{0.33}P_{0.33}O_4$ were synthesized by solid state reactions at 800 °C. Stoichiometric raw materials ($LiOH{\cdot}H_2O$, fumed SiO_2, β-Li_3PO_4, and $Al(OH)_3$) were first ball milled (zirconia beads/powder =12/1 in mass, 600 rpm, 12 h) in zirconia jars. The as-homogenized mixture was then cold-pressed into pellets and heated at 800 °C for 12 h under Ar flow, followed by slow cooling to 298 K and then grinding. The Si/Al/P relative concentrations in the powder were confirmed by energy dispersed X-ray (EDX) analysis. The crystal structure of these samples was studied by powder X-ray diffraction. Neutron powder diffraction patterns were collected for Li_4SiO_4, $Li_{3.75}Si_{0.75}P_{0.25}O_4$, and $Li_{4.25}Si_{0.75}Al_{0.25}O_4$ using the high-resolution D2B diffractometer at ILL (Institute Laue-Langevin, Grenoble, France). The ionic conductivity values were measured using pellet samples fabricated by the spark plasma sintering process (700 °C, 30 min) followed by gold sputtering on each plane surface. AC electrical impedance spectroscopy (EIS) measurements were performed under argon to avoid moisture at various stabilized temperatures ranging from 50 to 300 °C (upon heating and cooling with a step of 25 °C) using a Bio-Logic MTZ-35 Impedance Analyzer in a frequency range of 30 MHz to 0.1 Hz and with an excitation voltage of 0.1 V. From the Nyquist plots of the complex impedance data, the lithium ionic conductivities of the samples were derived.

2.2. Atomistic Modeling. Atomistic potential-based methods were used and are detailed elsewhere;[48,49] hence, only a brief overview is presented here. Molecular dynamics (MD) simulation of ion diffusion was performed with the LAMMPS code.[50,51] The interatomic potentials we used here include a long-range Coulomb term, a short-range Morse function, and a repulsive contribution. The parameters were taken from the extensive library of potentials developed by Pedone et al.,[52] which have been shown to perform well in MD simulations of silicates and polyanion-type materials. The mathematical form of the potentials and the values of the parameters are listed in the Supporting Information, Figure S1. On the basis of the crystal structure, we determined from single crystal X-ray diffraction and powder neutron diffraction that a supercell containing about 6000 atoms was generated. MD simulations were performed for long time scales (~3 ns) with a time step of 0.002 ps at a wide range of temperatures (473−1173 K). The mean squared displacement (MSD) of Li^+ ions was resolved, and the chemical diffusion coefficients (D_c) were then calculated from the relation: $D_c = \frac{1}{6}\frac{d\langle MSD\rangle}{dt}$. The tracer diffusion coefficients (D_t) were derived in a similar way using the mean displacement squared (MDS). The ionic conductivities were then calculated according to the Nernst−Einstein equation:

$$\frac{\sigma}{D_c} = \frac{nq^2}{fkT} \quad (1)$$

in which f is the Haven ratio defined as the ratio of D_c over D_t (their values are listed in the Supporting Information), n is the density of charge carrier (number of Li^+ ions per volume unit), q is the charge, k is the Boltzmann constant, and T is the system temperature. Such atomistic modeling techniques have been applied successfully to a range of lithium (and sodium) battery materials.[53−58]

3. RESULTS AND DISCUSSION

3.1. Crystal Structure of the LISICON-like Materials. The crystal structures of Li_4SiO_4, $Li_{3.75}Si_{0.75}P_{0.25}O_4$, $Li_{4.25}Si_{0.75}Al_{0.25}O_4$, and $Li_4Al_{0.33}Si_{0.33}P_{0.33}O_4$ were investigated using powder X-ray diffraction. The obtained diffraction patterns for the four samples are shown in Figure 2.

These four samples are well-crystallized and single phase. It is known that Li_4SiO_4 crystallizes in a monoclinic "supercell" (space group $P2_1/m$, no. 11) with Z = 14 at 298 K and undergoes a phase transition to a "subcell" with Z = 2 at temperatures higher than 750 K.[20,59,60] This transition is due to a disordering within the Li^+ crystallographic positions. This order−disorder transition in the Li^+ ion positions suggests that the diffusion mechanism may change with temperature. In contrast, the crystal structures at 298 K of the substituted compositions $Li_{3.75}Si_{0.75}P_{0.25}O_4$, $Li_{4.25}Si_{0.75}Al_{0.25}O_4$, and $Li_4Al_{0.33}Si_{0.33}P_{0.33}O_4$ can be described using the subcell model. The cell parameters obtained through full pattern profile matching are listed in Table 1.

The crystal structures can be described as isolated polyanionic tetrahedra (SiO_4, PO_4) connected to LiO_n (n = 4, 5, and 6) polyhedra through corner and/or edge sharing. For Li_4SiO_4 and $Li_{3.75}Si_{0.75}P_{0.25}O_4$, detailed structural descriptions were reported in previous studies.[20,61] In $Li_{3.75}Si_{0.75}P_{0.25}O_4$, the Si and P atoms share the same crystallographic sites, and $(SiO_4)^{4-}$ and $(PO_4)^{3-}$ coexist in a disordered manner.

DOI: 10.1021/acsami.6b14402
ACS Appl. Mater. Interfaces 2017, 9, 7050−7058

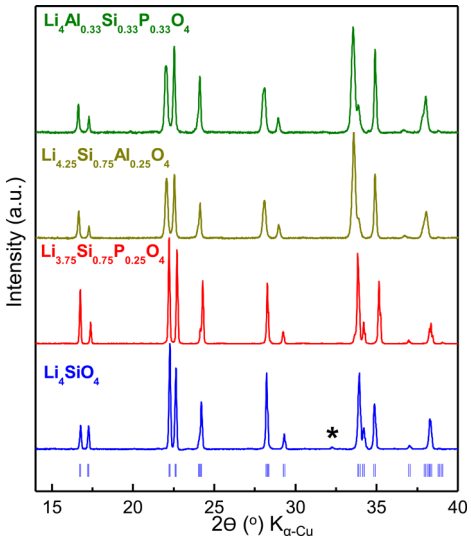

Figure 2. X-ray powder diffraction patterns for Li_4SiO_4 (blue), $Li_{3.75}Si_{0.75}P_{0.25}O_4$ (red), $Li_{4.25}Si_{0.75}Al_{0.25}O_4$ (dark yellow), and $Li_4Al_{0.33}Si_{0.33}P_{0.33}O_4$ (green). The Bragg positions of Li_4SiO_4 (subcell model) are shown in blue bars (* represents a superstructure reflection).

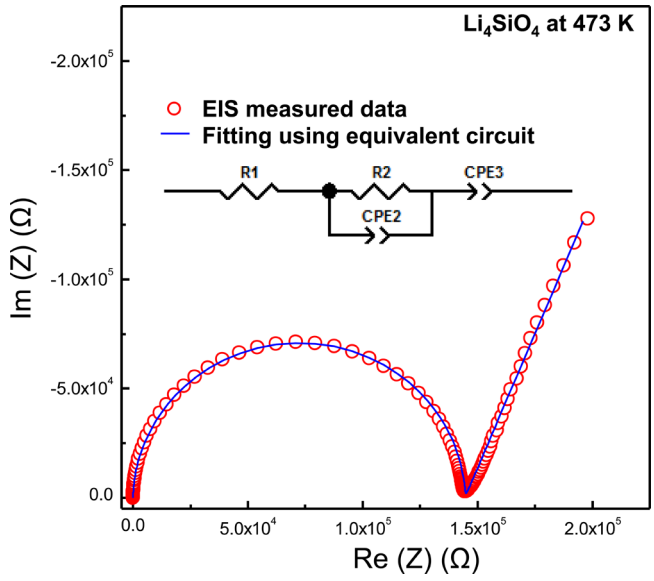

Figure 3. Nyquist plot for EIS measured data (red circles) and fitted curve (blue line) using the inserted equivalent circuit. The curve is obtained from measuring a Li_4SiO_4 pellet (h = 1.60 mm and S = 26.75 mm^2) at 473 K. The fitting was performed using the ZView software.

To the best of our knowledge, no investigation for the crystal structure of $Li_{4.25}Si_{0.75}Al_{0.25}O_4$ has been reported in the past. Ortiz-Landeros et al.[43] stated only that $Li_{4+x}Si_{1-x}Al_xO_4$ ($0 \leq x \leq 0.5$) compositions show an X-ray diffraction pattern very similar to that of Li_4SiO_4. In this work, we carried out powder neutron diffraction and single crystal X-ray diffraction for $Li_{4.25}Si_{0.75}Al_{0.25}O_4$. The refinement results of the crystal structure are listed in the Supporting Information. From neutron diffraction data, the refined lithium amount is 4.1(3) per formula. The crystal structure of $Li_{4.25}Si_{0.75}Al_{0.25}O_4$ is very similar to that of $Li_{3.75}Si_{0.75}P_{0.25}O_4$,[20] with a unit cell containing two XO_4 tetrahedra and similar distribution of lithium crystallographic sites. Each X site is statistically shared by 0.75 Si and 0.25 Al atoms. In the mixed XO_4 group, the average X−O bond length is 1.690 Å, which is very close to the value of 1.684 Å obtained by linear interpolation between the average Si−O distance in Li_4SiO_4 (1.641 Å) and Al−O distance in β-Li_5AlO_4 (1.814 Å) as reported by Hoppe et al.[62] This is a strong indication that the experimental Si/Al stoichiometry of the powder is very close to the nominal one and that the structural model we are using is valid.

3.2. Ionic Conductivity Enhancement by Mixing Tetrahedral Groups. The ionic conductivity of each material has been measured by EIS technique as a function of temperature. Figure 3 shows a typical Nyquist plot obtained for Li_4SiO_4 at 473 K.

A semicircle can be observed at high frequencies, which can be attributed to the solid electrolyte lithium ion conduction. The spectra were fitted by an equivalent circuit (insert in Figure 3) composed by an initial resistor R1 (for the device and current collectors resistance) in series with one resistor R2 (for solid electrolyte resistance) in parallel with a constant phase element CPE2 (for the nonideal capacitance between particles) and in series with another CPE3 (for the impedance of both the top and bottom electrode−electrolyte junctions). The ionic conductivity σ was then calculated using the equation:

$$\sigma = \frac{h}{RS} \tag{2}$$

in which h is the thickness of the solid electrolyte pellet, S the pellet surface, and R the resistance obtained from the fitted R2 value. A fast reduction of the semicircle diameter is noticed upon heating, in line with the enhancement of the ionic conductivity with temperature.

The ionic conductivities have also been calculated using the MD method described in detail in the Methods section. In Figure 4, the experimental and MD simulated ionic conductivity values of Li_4SiO_4, $Li_{3.75}Si_{0.75}P_{0.25}O_4$, $Li_{4.25}Si_{0.75}Al_{0.25}O_4$, $Li_4Al_{0.33}Si_{0.33}P_{0.33}O_4$, and $Li_4Al_{1/3}Si_{1/6}Ge_{1/6}P_{1/3}O_4$ are plotted in the form of log (σT) as a function of 1000/T.

For each composition, the EIS measured and the MD simulated ionic conductivity values are in good agreement and follow the expected Arrhenius relationship:

Table 1. Cell Parameters of Li_4SiO_4, $Li_{3.75}Si_{0.75}P_{0.25}O_4$, $Li_{4.25}Si_{0.75}Al_{0.25}O_4$, and $Li_4Al_{0.33}Si_{0.33}P_{0.33}O_4$ Obtained from Full Pattern Profile Matching of X-ray Powder Diffraction Data

	Li_4SiO_4	$Li_{3.75}Si_{0.75}P_{0.25}O_4$	$Li_{4.25}Si_{0.75}Al_{0.25}O_4$	$Li_4Al_{0.33}Si_{0.33}P_{0.33}O_4$
a (Å)	5.1497(2)	5.1084(1)	5.1496(2)	5.1475(3)
b (Å)	6.1001(2)	6.1126(2)	6.1771(4)	6.1779(5)
c (Å)	5.2981(2)	5.3020(2)	5.3424(2)	5.3497(3)
β (deg)	90.32(1)	90.34(1)	90.30(1)	90.34(1)
V/Z (Å^3)	83.21(1)	82.78(1)	84.97(1)	85.06(1)

DOI: 10.1021/acsami.6b14402
ACS Appl. Mater. Interfaces 2017, 9, 7050−7058

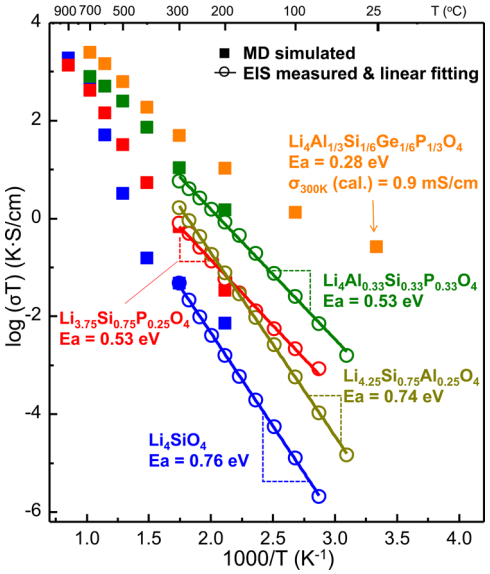

Figure 4. Li^+ ionic conductivity (σ), Arrhenius plots for Li_4SiO_4 (blue), $Li_{3.75}Si_{0.75}P_{0.25}O_4$ (red), $Li_{4.25}Si_{0.75}Al_{0.25}O_4$ (dark yellow), $Li_4Al_{0.33}Si_{0.33}P_{0.33}O_4$ (green), and $Li_4Al_{1/3}Si_{1/6}Ge_{1/6}P_{1/3}O_4$ (orange). MD simulated values are shown in solid squares. Conductivity values deduced from EIS measurements are shown in circles. Linear fits for experimental values are plotted in solid lines. The activation energies are derived in the temperature range of 50−300 °C.

$$\sigma T = A\exp\left(-\frac{Ea}{kT}\right) \quad (3)$$

where A is a pre-exponential factor related to charge carrier concentration and E_a is the activation energy. Li_4SiO_4 shows low ionic conductivity in the typical solid state battery working temperature range (RT to 473 K, with $\sigma_{473K} = 4.10^{-6}$ S/cm). In both mixed "binary" compositions, the ionic conductivity values are increased by 2 orders of magnitude with $\sigma_{473K} = 1.10^{-4}$ S/cm for $Li_{3.75}Si_{0.75}P_{0.25}O_4$ and 2.10^{-4} S/cm for $Li_{4.25}Si_{0.75}Al_{0.25}O_4$. A further enhancement of the ionic conductivity is seen in the "ternary" composition $Li_4Al_{0.33}Si_{0.33}P_{0.33}O_4$ with $\sigma_{473K} = 1.10^{-3}$ S/cm. These results indicate that substitution on the Si sites (thus creating either Li vacancies or Li^+ interstitial sites) can effectively promote lithium ion diffusivity. This conclusion is valid not only for the oxide LISICON type materials but also appears to be applicable for sulfide-based solid electrolytes.[25] It is significant that the MD simulated ionic conductivity of $Li_4Al_{1/3}Si_{1/6}Ge_{1/6}P_{1/3}O_4$ is as high as 0.9 mS/cm at 300 K, which is one of the highest values among oxide-based solid electrolytes.[29,46,63] We notice that the slopes of the data are not strictly linear in the temperature range of 300−1173 K, suggesting that the Li diffusion mechanism is temperature-dependent. Nevertheless, the non-Arrhenius behavior is consistent with the order−disorder transition in the Li^+ ion positions previously observed using diffraction techniques.

We now address the cause of this conductivity enhancement in substituted compositions. All of these compositions crystallize in the LISICON-like structure with isolated tetrahedra and a wide distribution of Li ions on their crystallographic sites. The crystal structure and Li distribution are the same in our MD simulations for these compositions; hence, the influence of structural differences and cation ordering is minimized, which allows us to focus on the effect arising from the mixing of the polyanion groups. In general, the presence of various polyanion groups in the structure improves cation mobility by lowering the energy barrier for Li^+ migration. A similar phenomenon has been observed in the $Li_2S-GeS_2-LiBr-LiI$ system:[44] the mixing of S^{2-}, I^-, and Br^- anions lowers the activation energy and improves cation mobility. The mechanism is termed as the mixed anion effect. As an analogue, the ionic conductivity enhancement in the Li_4SiO_4-related compositions can be termed as the mixed polyanion effect because the mixing anions are XO_4 groups.

To evaluate the influence of each type of polyanion group, several intrinsic structural and energy characteristics of XO_4 tetrahedra (X = Al^{3+}, Si^{4+}, Ge^{4+}, and P^{5+}) are listed in Table 2.

Table 2. Tetrahedral Anion Charge (m), X−O Distance in Li_mXO_4, X−O Dissociation Energy Values,[64] Li^+-$(XO_4)^{m-}$ Interaction Minimum Positions for Different Types of Tetrahedra

$(XO_4)^{m-}$	X−O distance (Å)	molar mass	X−O dissociation energy (eV)	Li^+-$(XO_4)^{m-}$ binding energy (eV)	Li^+-$(XO_4)^{m-}$ equilibrium distance (Å)
$(AlO_4)^{5-}$	1.814	91	5.03	−6.08	5.2
$(SiO_4)^{4-}$	1.641	92		−5.15	5.1
$(GeO_4)^{4-}$	1.760	137	6.99	−5.06	5.2
$(PO_4)^{3-}$	1.520	95	6.17	−4.07	5.0

Substitution of silicon can alter the properties of the polyanion groups and the lithium population in three main ways:

(1) Lithium carrier concentration: The tetrahedral anion charge m influences not only the interaction between the tetrahedral group and Li^+ ions but also the number of charge carriers per formula. For example, with the same amount of substitution (25%) on the Si site, $Li_{3.75}Si_{0.75}P_{0.25}O_4$ has 3.75 Li per formula, but $Li_{4.25}Si_{0.75}Al_{0.25}O_4$ has 4.25 Li per formula. In Figure 4, we can see that there is no significant difference in ionic conductivities between these two compositions. In comparison to the ionic conductivity values of other compositions, it seems that the variation of the concentration of charge carriers is not the key factor that helps to enhance conductivity values in the substituted compositions.

(2) Polyanion size: The X−O bond length gives a direct description of the size of the tetrahedra. For consistency, the bond length values listed in Table 2 are taken from the average bond length in the corresponding ortho-oxide: Al−O from β-Li_5AlO_4 (ICSD-16229),[62] Si−O from Li_4SiO_4 (ICSD-8222),[60] Ge−O from Li_4GeO_4 (ICSD-65177), and P−O from γ-Li_3PO_4 (ICSD-77095). From PO_4 to AlO_4, the X−O bond length extends by 20%, which gives a 73% expansion of the tetrahedron. In previous studies,[20,24,65−67] the contribution of the tetrahedral motion to the cation ionic conductivity has been discussed, known as the "paddle wheel effect". The tetrahedra motion is affected by its degree of distortion as well as its rotation. The distortion is represented by the X−O dissociation energy which describes the strength of the bond. The rotation is strongly related to the molar mass of the tetrahedral group. In the MD simulation study of LGPS,[24] the Li^+ mobility is reported to correlate with a 30° rotation of the GeS_4 and PS_4 groups.

DOI: 10.1021/acsami.6b14402
ACS Appl. Mater. Interfaces 2017, 9, 7050−7058

(3) Lithium potential energy surface: We calculated the interaction between a Li^+ ion and a $(XO_4)^{m-}$ group. In the calculation one Li^+ ion and one $(XO_4)^{m-}$ group were set in a 40 × 40 × 40 Å lattice. The lattice energy was calculated as a function of separation r and is plotted in Figure 5 for each $(XO_4)^{m-}$ group. The results illustrate

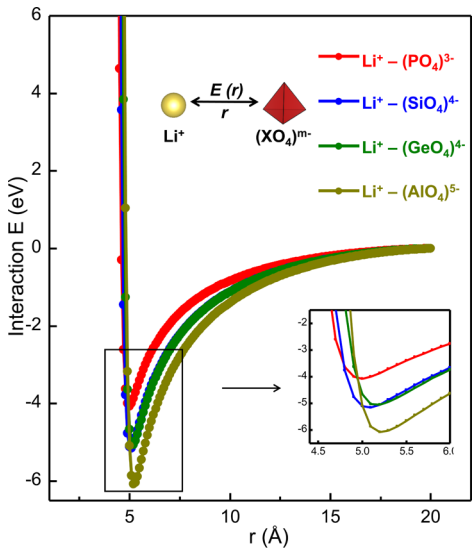

Figure 5. Simulated interaction between a Li^+ ion and different $(XO_4)^{m-}$ tetrahedral groups. The interaction includes a long-range Coulomb term, a short-range Morse function, and a repulsive contribution.

that the interaction between Li^+ and XO_4 can vary considerably in both the depth of the potential well and the equilibrium separation. The minimum energy value E_{min} shows a difference as large as 1 eV between Li^+-$(PO_4)^{3-}$ and Li^+-$(SiO_4)^{4-}$ and 2 eV between Li^+-$(PO_4)^{3-}$ and Li^+-$(AlO_4)^{5-}$. The equilibrium separation can vary by 0.25 Å.

The nonuniform potential wells for different Li^+-$(XO_4)^m$ interactions may modify the overall potential energy surface. In Li_4SiO_4, lithium occupies a much more uniform set of potential wells, and the activation energy is relatively high (0.76 eV). In the substituted compositions $Li_{3.75}Si_{0.75}P_{0.25}O_4$, $Li_{4.25}Si_{0.75}Al_{0.25}O_4$, $Li_4Al_{0.33}Si_{0.33}P_{0.33}O_4$, and $Li_4Al_{1/3}Si_{1/6}Ge_{1/6}P_{1/3}O_4$, the mixing of these XO_4 groups with their nonuniform potential wells may result in lower barriers between wells and reduced activation energies in the substituted compositions (0.53 eV for $Li_{3.75}Si_{0.75}P_{0.25}O_4$, 0.74 eV for $Li_{4.25}Si_{0.75}Al_{0.25}O_4$, and 0.53 eV for $Li_4Al_{0.33}Si_{0.33}P_{0.33}O_4$ from our EIS measurements). The calculated activation energy of 0.28 eV for $Li_4Al_{1/3}Si_{1/6}Ge_{1/6}P_{1/3}O_4$ is even lower.

3.3. Li^+ Diffusion Mechanism. To understand how the mixing of polyanion groups with different sizes and binding energies to Li^+ affects the conduction mechanisms, we performed statistical analysis of the lithium diffusion. In our previous study,[20] we showed that at 573 K, Li^+ diffusion in Li_4SiO_4 progresses via isolated Li^+ hops with a low conductivity of around 10^{-6} S/cm. By contrast, the substituted composition $Li_{3.5}Si_{0.5}P_{0.5}O_4$ displayed conductivity 3 orders of magnitude higher (10^{-3} S/cm) at the same temperature with Li^+ diffusion occurring via highly correlated motion. To further quantify these changes in diffusive behavior, we calculated and plotted the van Hove correlation functions for Li_4SiO_4, $Li_{3.75}Si_{0.75}P_{0.25}O_4$, and $Li_4Al_{1/3}Si_{1/6}Ge_{1/6}P_{1/3}O_4$ using trajectories obtained from our MD simulations, which can be split into the self-part G_s and the distinct-part G_d as follows:

$$G_s(r, t) = \frac{1}{4\pi r^2 N}\left\langle \sum_{i=1}^{N} \delta[r - |r_i(t_0) - r_i(t + t_0)|]\right\rangle_{t_0} \quad (4)$$

$$G_d(r, t) = \frac{1}{4\pi r^2 N}\left\langle \sum_{i\neq j}^{N} \delta[r - |r_i(t_0) - r_j(t + t_0)|]\right\rangle_{t_0} \quad (5)$$

In these two equations, the self-part G_s and the distinct-part G_d are functions of the Li^+–Li^+ pair distance r of the simulation time t. The angular brackets denote the ensemble average from the initial time t_0. N denotes the number of Li^+ ions in the system. $\delta()$ is the one-dimensional Dirac delta function. $r_i(t)$ denotes the position of the ith Li^+ ion at time t. For a given r and t, the self-part $G_s(r,t)$ or its transformed version $r^2G_s(r,t)$ is related to the probability of finding one atom after it travels a distance r after a time interval of t; the distinct-part $G_d(r,t)$ or its transformed version $r^2G_d(r,t)$ compares the positions of a particle to the position of another particle at different time and is related to the probability of finding atom j ($j \neq i$) with a distance r (compare to the position of atom i at t_0) after a time interval of t. In the particular case with $t = 0$, $G_d(r,t)$ is reduced to the static Li^+–Li^+ pair distribution function.

The transformed correlation function thus offers a measure of how correlated the motions of Li^+ ions are. If $r^2G_s(r,t)$ retains its shape over different time intervals, then noncorrelated ion hopping is indicated, whereas peak broadening indicates correlated motion, disorder on the Li^+ sublattice and, in extreme cases, liquid-like diffusive behavior. This method has been successfully used to investigate the diffusion mechanism in other ion conducting materials such as Na_3PS_4[68] and garnet-type $Li_{7-x}La_3(Zr_{2-x}M_x)O_{12}$[69] but has never been applied to LISICON systems.

In Figure 6, the transformed version of the self-part, $r^2G_s(r,t)$, is plotted as a function of r for Li_4SiO_4 and $Li_4Al_{1/3}Si_{1/6}Ge_{1/6}P_{1/3}O_4$ at various simulation temperatures (373, 573, 773, and 973 K) (The $r^2G_s(r,t)$ for $Li_{3.75}Si_{0.75}P_{0.25}O_4$ and the $r^2G_d(r,t)$ for the three compositions can be found in the Supporting Information). For each temperature, six time interval values, t = 1, 10, 50, 100, 250, and 500 ps, were chosen to investigate the structural dynamics evolution. From these simulated data, we can classify three distinct types of diffusive behavior according to the shape of $r^2G_s(r,t) = f(r)$ and $r^2G_s(r,t) = g(r)$.

Type I: Local Oscillation. Li_4SiO_4 at 373 K (Figure 6a) and 573 K (Figure 6b) and $Li_4Al_{1/3}Si_{1/6}Ge_{1/6}P_{1/3}O_4$ at 373 K (Figure 6e): the calculated data show only one peak appearing between 0 and 0.5 Å. This peak suggests a high probability of finding lithium ions with this displacement value; this probability shows weak time dependence. Such a correlation function is typical of atomic vibrations around equilibrium positions. This finding is in good agreement with the result found in the density plot of MD simulations in our previous work.[20] This peak also appears in the other plots of Figure 6 (and is listed in Table 3). As the temperature increases, a right shift of the peak position is observed, which is in agreement with the fact that the Li^+ ions have higher thermal energy at higher temperatures.

DOI: 10.1021/acsami.6b14402
ACS Appl. Mater. Interfaces 2017, 9, 7050–7058

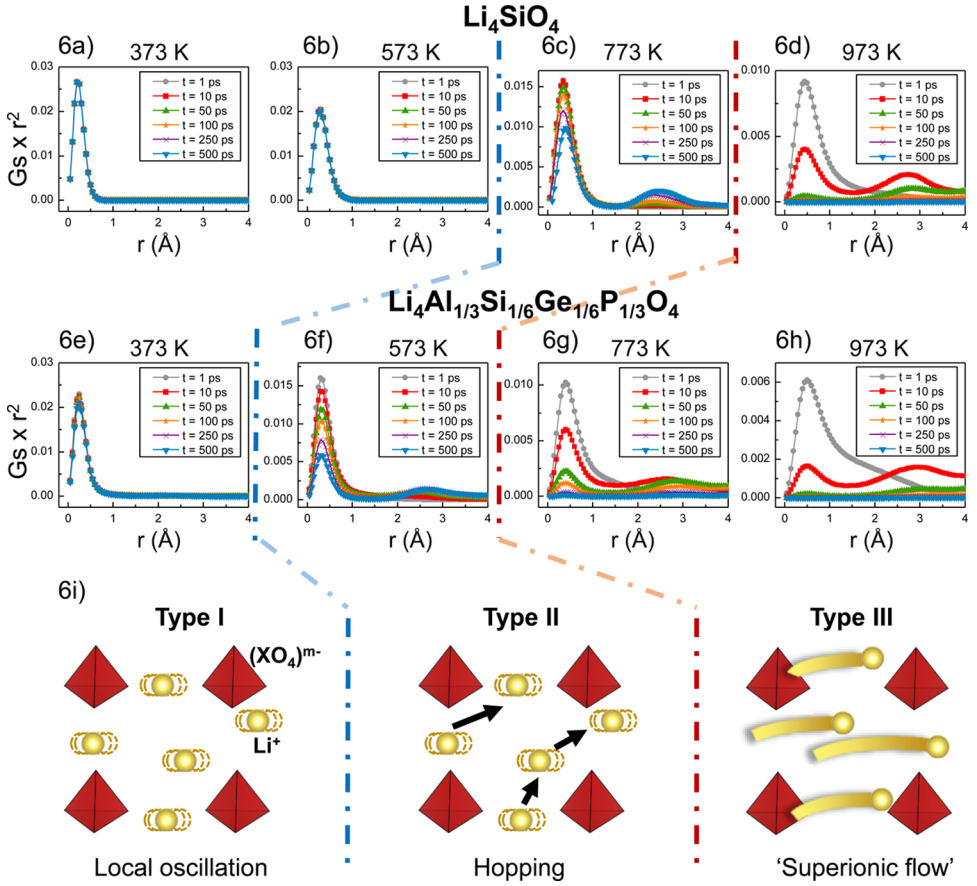

Figure 6. Transformed version of the self-part of the van Hove correlation function $r^2G_s(r,t)$ for Li_4SiO_4 (a–d) and $Li_4Al_{1/3}Si_{1/6}Ge_{1/6}P_{1/3}O_4$ (e–h) at (from left to right) 373, 573, 773, and 973 K. For each temperature, six curves for t = 1, 10, 50, 100, 250, and 500 ps are plotted. At each temperature, the six curves indicate one of the three mechanism types as shown in (i). Li^+ ions are shown in yellow; XO_4 groups are shown in red.

Table 3. First Peak Position (Å) in the Self-Part of the van Hove Correlation Function

	373 K	573 K	773 K	973 K
Li_4SiO_4	0.20	0.30	0.35	0.45
$Li_4Al_{1/3}Si_{1/6}Ge_{1/6}P_{1/3}O_4$	0.25	0.30	0.40	0.50

At each temperature, the peak position for $Li_4Al_{1/3}Si_{1/6}Ge_{1/6}P_{1/3}O_4$ appears at an r value slightly larger than that for Li_4SiO_4, indicating that the motion of Li^+ ions is less constricted. The mechanism of Li^+ ion dynamics in these cases can be considered as a local oscillation.

Type II: Ion Hopping. For Li_4SiO_4 at 773 K (Figure 6c) and $Li_4Al_{1/3}Si_{1/6}Ge_{1/6}P_{1/3}O_4$ at 573 K (Figure 6f), the intensity of the probability peak around 0.40 Å decreases with the evolution of the simulation time. Therefore, the probability of finding a Li^+ ion around its equilibrium position is reduced, indicating that Li^+ ions have left their original position and migrated to other sites. Another feature in these Type II plots is the presence of a second peak at around r = 2.4 Å, which is the distance between a Li^+ ion and its closest Li^+ site in the lattice (varying from 1.8 to 2.9 Å). The appearance of this peak is the signal for Li^+ ion jumping to its neighboring site and staying on that site for a certain residual time. Similar to the peak at 0.40 Å, this peak is also time dependent, but its intensity increases with the measurement interval. For time-scales greater than ~100 ps, sufficient Li^+ hops occur to give an appreciable probability of finding a Li^+ ion on its neighboring site. The hopping can also be seen in the distinct-part of the van Hove correlation function (see the Supporting Information). In the distinct-part curve, there is a peak locating at around 0.4 Å, suggesting that the lithium sites are occupied by a new Li^+ ion other than the one at t = 0. These features suggest that Li^+ ion diffusion undergoes a hopping mechanism in the type II conditions.

Type III: Correlated Superionic Flow. Li_4SiO_4 at 973 K (Figure 6d) and $Li_4Al_{1/3}Si_{1/6}Ge_{1/6}P_{1/3}O_4$ at 773 K (Figure 6g) and 973 K (Figure 6h): In these type III plots, those curves at t = 1 ps have shapes similar to those in the type I plots. However, the intensity of the peak is much weaker (it should be noted that the scales of the vertical axis are not same), indicating a lower probability of finding a Li^+ ion around its original position. The peak has a large tail, showing that some of the Li^+ ions are displaced for distances larger than 1.5 Å in 1 ps. The curves at t = 10 ps are similar to those in the type II plots with a relatively low intensity peak at 0.4 Å and a broad peak at 2.8 Å, suggesting that in these conditions, 10 ps is long enough for a Li^+ ion to diffuse to its neighboring site. As the simulation time goes above 100 ps, no other significant peaks can be observed in these plots.

These data show that at high temperatures, a significant disordering of the Li^+ sublattice in the structure occurs, which leads to a more liquid-like distribution of Li^+ ions. The diffusivity of the Li^+ ions at these temperatures is significantly enhanced, leading to the nonlinear Arrhenius behavior in the conductivity values in Figure 4. The Li^+ dynamics can thus be considered to undergo a phase transition into "superionic flow".

DOI: 10.1021/acsami.6b14402
ACS Appl. Mater. Interfaces 2017, 9, 7050–7058

The discussion above indicates that the mechanism of Li^+ ion diffusion in each composition is temperature-dependent. From low to high temperature, the mechanism evolves from type I local oscillation to type II isolated hopping and to type III superionic flow. When the diffusion mechanism changes from local oscillation to isolated hopping or isolated hopping to superionic flow, a faster Li^+ ion mobility is achieved, thus promoting higher ionic conductivity. The mixed polyanion effect causes substituted compositions to show a transition to the next diffusion mechanism type at a temperature much lower than that in Li_4SiO_4. For instance, $Li_4Al_{1/3}Si_{1/6}Ge_{1/6}P_{1/3}O_4$ shows a transition to superionic motion at a temperature much lower than that for Li_4SiO_4; hence, the room temperature conductivity is several orders of magnitude greater. In general, these results indicate the atomic scale origin of the orders of magnitude increase in ionic conductivity observed in substituted LISICON materials.

4. CONCLUSIONS

The lithium ion transport properties of a range of compositions (Li_4SiO_4, $Li_{3.75}Si_{0.75}P_{0.25}O_4$, $Li_{4.25}Si_{0.75}Al_{0.25}O_4$, $Li_4Al_{0.33}Si_{0.33}P_{0.33}O_4$, and $Li_4Al_{1/3}Si_{1/6}Ge_{1/6}P_{1/3}O_4$) in the LISICON-type structural family were investigated using a combination of synthesis, diffraction, impedance, and modeling techniques. This includes the first detailed report of the crystal structure, including atomic positions and site occupancies of $Li_{4.25}Si_{0.75}Al_{0.25}O_4$ and the transport properties of a new composition $Li_4Al_{0.33}Si_{0.33}P_{0.33}O_4$.

The following main findings emerge from our investigation. First, the ionic conductivity of Li_4SiO_4 is not high but can be enhanced through successful substitution on the Si^{4+} site. Such doping leads to a mixed polyanion effect which helps to modify the potential energy surface and decrease the Li^+ ion conduction barrier. Second, the MD modeling results reveal three temperature-dependent mechanisms for Li^+ ion diffusion: (i) local oscillation at low temperature, (ii) isolated hopping at intermediate temperature, and (iii) superionic motion at high temperature. Moreover, we showed that the type of mechanism in operation depends on both the temperature and composition. $Li_4Al_{1/3}Si_{1/6}Ge_{1/6}P_{1/3}O_4$ shows a transition to superionic motion at a temperature much lower than that of Li_4SiO_4; hence, the room temperature ionic conductivity of 0.9 mS/cm is several orders of magnitude higher. The results are generally applicable to all materials in the LISICON family, which share the same structural motif of Li-rich compounds with isolated polyanion tetrahedra.

These insights are important to rationalize how ionic transport is related to local structure and composition, and to develop new strategies for designing solid electrolyte materials with high ionic conductivity. A future avenue to exploit this effect would be mixed oxysulfide compositions where the size difference in tetrahedra would be even greater than that in the oxides considered here, although a major challenge presented by such oxysulfides (and by substituted LISICONs in general) is the suppression of phase separation.

ASSOCIATED CONTENT

Supporting Information

The Supporting Information is available free of charge on the ACS Publications website at DOI: 10.1021/acsami.6b14402.

Equation and values of parameters used in the interatomic potentials, self-part of the van Hove correlation function for $Li_{3.75}Si_{0.75}P_{0.25}O_4$, distinct-part of the van Hove correlation function, single crystal measurement conditions and refinement results, Haven ratio values, crystallographic data, and powder neutron diffraction pattern for $Li_{4.25}Si_{0.75}Al_{0.25}O_4$ (PDF)

AUTHOR INFORMATION

Corresponding Authors

*E-mail: christian.masquelier@u-picardie.fr.
*E-mail: m.s.islam@bath.ac.uk.

ORCID

Christopher Eames: 0000-0002-5548-2655
Christian Masquelier: 0000-0001-7289-1015

Notes

The authors declare no competing financial interest.

ACKNOWLEDGMENTS

The ALISTORE ERI and the CNRS are acknowledged for supporting Y.D. through a joint Ph.D. scholarship between Amiens (France) and Bath (U.K.). We acknowledge the support from the EPSRC for the Energy Materials Programme grant (EP/K016288) and Archer HPC facilities through the Materials Chemistry Consortium (EP/L000202).

REFERENCES

(1) Armand, M.; Tarascon, J.-M. Building Better Batteries. *Nature* **2008**, *451*, 652−657.
(2) Scrosati, B.; Garche, J. Lithium Batteries: Status, Prospects and Future. *J. Power Sources* **2010**, *195*, 2419−2430.
(3) Simon, P.; Gogotsi, Y. Materials for Electrochemical Capacitors. *Nat. Mater.* **2008**, *7*, 845−854.
(4) Goodenough, J. B. Rechargeable Batteries: Challenges Old and New. *J. Solid State Electrochem.* **2012**, *16*, 2019−2029.
(5) Winter, M.; Brodd, R. J. What Are Batteries, Fuel Cells, and Supercapacitors? *Chem. Rev.* **2004**, *104*, 4245−4270.
(6) Kamaya, N.; Homma, K.; Yamakawa, Y.; Hirayama, M.; Kanno, R.; Yonemura, M.; Kamiyama, T.; Kato, Y.; Hama, S.; Kawamoto, K.; Mitsui, A. A Lithium Superionic Conductor. *Nat. Mater.* **2011**, *10*, 682−686.
(7) Masquelier, C. Solid Electrolytes: Lithium Ions on the Fast Track. *Nat. Mater.* **2011**, *10*, 649−650.
(8) Quartarone, E.; Mustarelli, P. Electrolytes for Solid-State Lithium Rechargeable Batteries: Recent Advances and Perspectives. *Chem. Soc. Rev.* **2011**, *40*, 2525−2540.
(9) Fergus, J. W. Ceramic and Polymeric Solid Electrolytes for Lithium-Ion Batteries. *J. Power Sources* **2010**, *195*, 4554−4569.
(10) Kanno, R.; Murayama, M. Lithium Ionic Conductor Thio-LISICON: The Li_2S-GeS_2-P_2S_5 System. *J. Electrochem. Soc.* **2001**, *148*, A742−A746.
(11) Mizuno, F.; Hayashi, A.; Tadanaga, K.; Tatsumisago, M. New, Highly Ion-Conductive Crystals Precipitated from Li_2S−P_2S_5 Glasses. *Adv. Mater.* **2005**, *17*, 918−921.
(12) Li, J.; Ma, C.; Chi, M.; Liang, C.; Dudney, N. J. Lithium-Ion Batteries: Solid Electrolyte: The Key for High-Voltage Lithium Batteries. *Adv. Energy Mater.* **2015**, *5*, 1401408.
(13) Goodenough, J. B.; Hong, H. Y.-P.; Kafalas, J. A. Fast Na^+-Ion Transport in Skeleton Structures. *Mater. Res. Bull.* **1976**, *11*, 203−220.
(14) Roy, S.; Kumar, P. P. Influence of Cationic Ordering on Ion Transport in NASICONs: Molecular Dynamics Study. *Solid State Ionics* **2013**, *253*, 217−222.
(15) Guin, M.; Tietz, F. Survey of the Transport Properties of Sodium Superionic Conductor Materials for Use in Sodium Batteries. *J. Power Sources* **2015**, *273*, 1056−1064.

(16) Susman, S.; Delbecq, C. J.; Brun, T. O.; Prince, E. Fast Ion Transport in the NASICON Analog $Na_3Sc_2(PO_4)_3$: Structure and Conductivity. *Solid State Ionics* **1983**, *9−10*, 839−844.
(17) Song, S.; Lu, J.; Zheng, F.; Duong, H. M.; Lu, L. A Facile Strategy to Achieve High Conduction and Excellent Chemical Stability of Lithium Solid Electrolytes. *RSC Adv.* **2015**, *5*, 6588−6594.
(18) Hu, Y.-W.; Raistrick, I. D.; Huggins, R. A. Ionic Conductivity of Lithium Orthosilicate—Lithium Phosphate Solid Solutions. *J. Electrochem. Soc.* **1977**, *124*, 1240−1242.
(19) Shannon, R. D.; Taylor, B. E.; English, A. D.; Berzins, T. New Li Solid Electrolytes. *Electrochim. Acta* **1977**, *22*, 783−796.
(20) Deng, Y.; Eames, C.; Chotard, J.-N.; Lalère, F.; Seznec, V.; Emge, S.; Pecher, O.; Grey, C. P.; Masquelier, C.; Islam, M. S. Structural and Mechanistic Insights into Fast Lithium-Ion Conduction in Li_4SiO_4−Li_3PO_4 Solid Electrolytes. *J. Am. Chem. Soc.* **2015**, *137*, 9136−9145.
(21) Masquelier, C.; Kageyama, H.; Takeuchi, T.; Saito, Y.; Nakamura, O. Chemistry and Structure Analysis in the $Li_{4+x}B_xSi_{1-x}O_4$ Solid Solution. *J. Power Sources* **1995**, *54*, 448−451.
(22) Kuhn, A.; Gerbig, O.; Zhu, C.; Falkenberg, F.; Maier, J.; Lotsch, B. V. A New Ultrafast Superionic Li-Conductor: Ion Dynamics in $Li_{11}Si_2PS_{12}$ and Comparison with Other Tetragonal LGPS-Type Electrolytes. *Phys. Chem. Chem. Phys.* **2014**, *16*, 14669−14674.
(23) Bron, P.; Johansson, S.; Zick, K.; Schmedt auf der Günne, J.; Dehnen, S.; Roling, B. $Li_{10}SnP_2S_{12}$: An Affordable Lithium Superionic Conductor. *J. Am. Chem. Soc.* **2013**, *135*, 15694−15697.
(24) Adams, S.; Rao, R. P. Structural Requirements for Fast Lithium Ion Migration in $Li_{10}GeP_2S_{12}$. *J. Mater. Chem.* **2012**, *22* (16), 7687−7691.
(25) Kato, Y.; Hori, S.; Saito, T.; Suzuki, K.; Hirayama, M.; Mitsui, A.; Yonemura, M.; Iba, H.; Kanno, R. High-Power All-Solid-State Batteries Using Sulfide Superionic Conductors. *Nat. Energy.* **2016**, *1*, 16030.
(26) Klenk, M.; Lai, W. Local Structure and Dynamics of Lithium Garnet Ionic Conductors: Tetragonal and Cubic $Li_7La_3Zr_2O_7$. *Phys. Chem. Chem. Phys.* **2015**, *17*, 8758−8768.
(27) Xia, W.; Xu, B.; Duan, H.; Guo, Y.; Kang, H.; Li, H.; Liu, H. Ionic Conductivity and Air Stability of Al-Doped $Li_7La_3Zr_2O_{12}$ Sintered in Alumina and Pt Crucibles. *ACS Appl. Mater. Interfaces* **2016**, *8*, 5335−5342.
(28) Tan, G.; Wu, F.; Zhan, C.; Wang, J.; Mu, D.; Lu, J.; Amine, K. Solid-State Li-Ion Batteries Using Fast, Stable, Glassy Nanocomposite Electrolytes for Good Safety and Long Cycle-Life. *Nano Lett.* **2016**, *16*, 1960−1968.
(29) Bachman, J. C.; Muy, S.; Grimaud, A.; Chang, H.-H.; Pour, N.; Lux, S. F.; Paschos, O.; Maglia, F.; Lupart, S.; Lamp, P.; Giordano, L.; Shao-Horn, Y. Inorganic Solid-State Electrolytes for Lithium Batteries: Mechanisms and Properties Governing Ion Conduction. *Chem. Rev.* **2016**, *116*, 140−162.
(30) Rao, R. P.; Sharma, N.; Peterson, V. K.; Adams, S. Formation and Conductivity Studies of Lithium Argyrodite Solid Electrolytes Using in-Situ Neutron Diffraction. *Solid State Ionics* **2013**, *230*, 72−76.
(31) Lopez-Bermudez, B.; Zeier, W. G.; Zhou, S.; Lehner, A. J.; Hu, J.; Scanlon, D. O.; Morgan, B. J.; Melot, B. C. Lithium-Ion Conductivity in $Li_6Y(BO_3)_3$: A Thermally and Electrochemically Robust Solid Electrolyte. *J. Mater. Chem. A* **2016**, *4*, 6972−6979.
(32) Mani, P. D.; Saraf, S.; Singh, V.; Real-Robert, M.; Vijayakumar, A.; Duranceau, S. J.; Seal, S.; Coffey, K. R. Ionic Conductivity of Bias Sputtered Lithium Phosphorus Oxy-Nitride Thin Films. *Solid State Ionics* **2016**, *287*, 48−59.
(33) Wenzel, S.; Randau, S.; Leichtweiß, T.; Weber, D. A.; Sann, J.; Zeier, W. G.; Janek, J. Direct Observation of the Interfacial Instability of the Fast Ionic Conductor $Li_{10}GeP_2S_{12}$ at the Lithium Metal Anode. *Chem. Mater.* **2016**, *28*, 2400−2407.
(34) Han, F.; Gao, T.; Zhu, Y.; Gaskell, K. J.; Wang, C. A Battery Made from a Single Material. *Adv. Mater.* **2015**, *27*, 3473−3483.
(35) Whiteley, J. M.; Woo, J. H.; Hu, E.; Nam, K.-W.; Lee, S.-H. Empowering the Lithium Metal Battery through a Silicon-Based Superionic Conductor. *J. Electrochem. Soc.* **2014**, *161*, A1812−A1817.
(36) Masquelier, C.; Tabuchi, M.; Takeuchi, T.; Soizumi, W.; Kageyama, H.; Nakamura, O. Influence of the Preparation Process on the Cation Transport Properties of $Li_{4+x}M_xSi_{1-x}O_4$ (M = B, Al) Solid Electrolytes. *Solid State Ionics* **1995**, *79*, 98−105.
(37) Saito, Y.; Ado, K.; Asai, T.; Kageyama, H.; Nakamura, O. Conductivity Enhancement Mechanism of Interstitial-Type Li^+ Conductor, $Li_{4+x}B_xSi_{1-x}$ ($0 \leq \times \leq 0.7$). *Solid State Ionics* **1991**, *47*, 149−154.
(38) Saito, Y.; Asai, T.; Ado, K.; Kageyama, H.; Nakamura, O. Ionic Conductivity of Li^+ Ion Conductors, $Li_{4.2}M_xSi_{1-x}O_4$ (M: B^{3+}, Al^{3+}, Ga^{3+}, Cr^{3+}, Fe^{3+}, Co^{2+}, Ni^{2+}). *Solid State Ionics* **1990**, *40−41*, 34−37.
(39) Tatsumisago, M.; Takano, R.; Tadanaga, K.; Hayashi, A. Preparation of Li_3BO_3−Li_2SO_4 Glass−ceramic Electrolytes for All-Oxide Lithium Batteries. *J. Power Sources* **2014**, *270*, 603−607.
(40) Sakurai, Y.; Sakuda, A.; Hayashi, A.; Tatsumisago, M. Preparation of Amorphous Li_4SiO_4−Li_3PO_4 Thin Films by Pulsed Laser Deposition for All-Solid-State Lithium Secondary Batteries. *Solid State Ionics* **2011**, *182*, 59−63.
(41) Neudecker, B. J.; Weppner, W. Li_9SiAlO_8: A Lithium Ion Electrolyte for Voltages above 5.4 V. *J. Electrochem. Soc.* **1996**, *143*, 2198−2203.
(42) Stebbins, J. F.; Xu, Z.; Vollath, D. Cation Exchange Rates and Mobility in Aluminum-Doped Lithium Orthosilicate: High-Resolution Lithium-6 NMR Results. *Solid State Ionics* **1995**, *78*, L1−L8.
(43) Ortiz-Landeros, J.; Gómez-Yáñez, C.; Palacios-Romero, L. M.; Lima, E.; Pfeiffer, H. Structural and Thermochemical Chemisorption of CO_2 on $Li_{4+x}(Si_{1-x}Al_x)O_4$ and $Li_{4-x}(Si_{1-x}V_x)O_4$ Solid Solutions. *J. Phys. Chem. A* **2012**, *116*, 3163−3171.
(44) Carette, B.; Ribes, M.; Souquet, J. L. The Effects of Mixed Anions in Ionic Conductive Glasses. *Solid State Ionics* **1983**, *9*, 735−737.
(45) Gundusharma, U. M.; Secco, E. A. New Positive Mixed Alkali and Mixed Anion Effects on Fast Na^+ Ion Conductivity in Na_2SO_4. *Can. J. Chem.* **1987**, *65*, 1205−1208.
(46) Tatsumisago, M.; Nagao, M.; Hayashi, A. Recent Development of Sulfide Solid Electrolytes and Interfacial Modification for All-Solid-State Rechargeable Lithium Batteries. *J. Asian Ceram. Soc.* **2013**, *1*, 17−25.
(47) Suzuki, K.; Nakamura, Y.; Tanibata, N.; Hayashi, A.; Tatsumisago, M. Preparation and Characterization of Na_3BO_3−Na_2SO_4 Glass Electrolytes with Na^+ Ion Conductivity Prepared by a Mechanical Milling Technique. *J. Asian Ceram. Soc.* **2016**, *4*, 6−10.
(48) Catlow, C. R. A. *Computer Modelling in Inorganic Crystallography*; Academic Press: San Diego; Boston, 1997.
(49) Islam, M. S.; Fisher, C. A. J. Lithium and Sodium Battery Cathode Materials: Computational Insights into Voltage, Diffusion and Nanostructural Properties. *Chem. Soc. Rev.* **2014**, *43*, 185−204.
(50) Plimpton, S. Fast Parallel Algorithms for Short-Range Molecular Dynamics. *J. Comput. Phys.* **1995**, *117*, 1−19.
(51) LAMMPS Molecular Dynamics Simulator http://lammps.sandia.gov/index.html (accessed July 15, 2016).
(52) Pedone, A.; Malavasi, G.; Menziani, M. C.; Cormack, A. N.; Segre, U. A New Self-Consistent Empirical Interatomic Potential Model for Oxides, Silicates, and Silica-Based Glasses. *J. Phys. Chem. B* **2006**, *110*, 11780−11795.
(53) Islam, M. S.; Driscoll, D. J.; Fisher, C. A. J.; Slater, P. R. Atomic-Scale Investigation of Defects, Dopants, and Lithium Transport in the $LiFePO_4$ Olivine-Type Battery Material. *Chem. Mater.* **2005**, *17*, 5085−5092.
(54) Tripathi, R.; Wood, S. M.; Islam, M. S.; Nazar, L. F. Na-Ion Mobility in Layered Na_2FePO_4F and Olivine $Na[Fe,Mn]PO_4$. *Energy Environ. Sci.* **2013**, *6*, 2257−2264.
(55) Clark, J. M.; Nishimura, S.; Yamada, A.; Islam, M. S. High-Voltage Pyrophosphate Cathode: Insights into Local Structure and Lithium-Diffusion Pathways. *Angew. Chem., Int. Ed.* **2012**, *51*, 13149−13153.
(56) Armstrong, A. R.; Lyness, C.; Panchmatia, P. M.; Islam, M. S.; Bruce, P. G. The Lithium Intercalation Process in the Low-Voltage Lithium Battery Anode $Li_{1+x}V_{1-x}O_2$. *Nat. Mater.* **2011**, *10*, 223−229.

DOI: 10.1021/acsami.6b14402
ACS Appl. Mater. Interfaces 2017, 9, 7050−7058

(57) Clark, J. M.; Eames, C.; Reynaud, M.; Rousse, G.; Chotard, J.-N.; Tarascon, J.-M.; Islam, M. S. High Voltage Sulphate Cathodes $Li_2M(SO_4)_2$ (M = Fe, Mn, Co): Atomic-Scale Studies of Lithium Diffusion, Surfaces and Voltage Trends. *J. Mater. Chem. A* **2014**, *2*, 7446−7453.
(58) Armstrong, A. R.; Kuganathan, N.; Islam, M. S.; Bruce, P. G. Structure and Lithium Transport Pathways in Li_2FeSiO_4 Cathodes for Lithium Batteries. *J. Am. Chem. Soc.* **2011**, *133*, 13031−13035.
(59) Duan, Y.; Parlinski, K. Density Functional Theory Study of the Structural, Electronic, Lattice Dynamical, and Thermodynamic Properties of Li_4SiO_4 and Its Capability for CO_2 Capture. *Phys. Rev. B: Condens. Matter Mater. Phys.* **2011**, *84*, 104113.
(60) Tranqui, D.; Shannon, R. D.; Chen, H. Y.; Iijima, S.; Baur, W. H. Crystal Structure of Ordered Li_4SiO_4. *Acta Crystallogr., Sect. B: Struct. Crystallogr. Cryst. Chem.* **1979**, *35*, 2479−2487.
(61) Baur, W. H.; Ohta, T. The Crystal Structure of $Li_{3.75}Si_{0.75}P_{0.25}O_4$ and Ionic Conductivity in Tetrahedral Structures. *J. Solid State Chem.* **1982**, *44*, 50−59.
(62) Hoppe, R.; König, H. Zur Kristallstruktur von β-Li_5AlO_4. *Z. Anorg. Allg. Chem.* **1977**, *430*, 211−217.
(63) Li, J.; Ma, C.; Chi, M.; Liang, C.; Dudney, N. J. Solid Electrolyte: The Key for High-Voltage Lithium Batteries. *Adv. Energy Mater.* **2015**, *5*, 1401408.
(64) National Standard Reference Data Series (NSRDS) http://nvlpubs.nist.gov/nistpubs/Legacy/NSRDS/nbsnsrds31.pdf (accessed February 4, 2017).
(65) Burmakin, E. I.; Shekhtman, G. S. On Ion Transport Mechanism in K^+-Conducting Solid Electrolytes Based on K_3PO_4. *Solid State Ionics* **2014**, *265*, 46−48.
(66) Yin, W.-G.; Liu, J.; Duan, C.-G.; Mei, W.; Smith, R.; Hardy, J. Superionicity in Na_3PO_4: A Molecular Dynamics Simulation. *Phys. Rev. B: Condens. Matter Mater. Phys.* **2004**, *70*, 64302.
(67) Jansen, M. Volume Effect or Paddle-Wheel Mechanism—Fast Alkali-Metal Ionic Conduction in Solids with Rotationally Disordered Complex Anions. *Angew. Chem., Int. Ed. Engl.* **1991**, *30*, 1547−1558.
(68) Zhu, Z.; Chu, I.-H.; Deng, Z.; Ong, S. P. Role of Na^+ Interstitials and Dopants in Enhancing the Na^+ Conductivity of the Cubic Na_3PS_4 Superionic Conductor. *Chem. Mater.* **2015**, *27*, 8318−8325.
(69) Adams, S.; Rao, R. P. Ion Transport and Phase Transition in $Li_{7-x}La_3(Zr_{2-x}M_x)O_{12}$ (M = Ta^{5+}, Nb^{5+}, X = 0, 0.25). *J. Mater. Chem.* **2012**, *22*, 1426−1434.

DOI: 10.1021/acsami.6b14402
ACS Appl. Mater. Interfaces 2017, 9, 7050−7058